Fuel 365 (2024) 131205

Contents lists available at ScienceDirect

Fuel

journal homepage: www.elsevier.com/locate/fuel

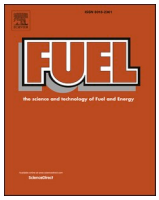

Full Length Article

Parametric and sensitive analysis of Pd-Ag membrane reactor performance in biogas reforming to generate decarbonized hydrogen by Computational Fluid Dynamic-Response Surface Methodology

K. Ghasemzadeh [a,b,*], T. Torabi [b], T. Yousefi Amiri [c], A. Fortunelli [d], A. Iulianelli [e,*]

[a] Department of Chemical Engineering, University of Manchester, M13 9PL Manchester, UK
[b] Department of Chemical Engineering, Urmia University of Technology, Urmia, Iran
[c] Department of Chemical Engineering, University of Zanjan, Zanjan, Iran
[d] ICCOM-CNR, Area Della Ricerca CNR di Pisa, Via Moruzzi 1, Pisa, 56124, Italy
[e] ITM-CNR, Via P. Bucci 17C, Rende (CS), 87036, Italy

ARTICLE INFO

Keywords:
Biogas steam reforming
Hydrogen production
Pd-Ag membrane reactor
CFD simulation
RSM analysis

ABSTRACT

The efficient production of hydrogen from renewable sources is pivotal for the development of sustainable energy systems. Biogas steam reforming (BSR) conducted in palladium-based membrane reactors (MRs) offers a pathway for high-purity H_2 generation at lower temperatures compared to traditional processes. In this study, a computational fluid dynamics (CFD) model was developed to simulate the BSR process within a Pd-Ag MR. The CFD model has integrated comprehensive kinetics, mass transport, and hydrodynamics, and its accuracy was confirmed through validation against experimental data, demonstrating substantial agreement. As a novel approach, to optimize the BSR reaction conditions to get the best MR performance, the CFD model was coupled with response surface methodology (RSM), which has been employed to enable the identification of optimal values for key parameters such as reaction temperature, pressure, gas hour space velocity, feed molar ratio, and sweep gas ratio, where the temperature was found to have the most significant impact on the MR's performance within the examined intervals of input parameters. The objective of RSM method applied to CFD modeling was to maximize with high accuracy CH_4 conversion, H_2 recovery, and reduce CO_2 emissions. RSM models effectively established correlations between input parameters and responses. The determined optimal conditions for the BSR process were a temperature of 683 K, a reaction pressure of 6 bar, a GHSV of 3000 h^{-1}, a H_2O/CH_4 ratio of 1.34, and a sweep ratio of 9. Under these conditions, the system achieved remarkable results with 100 % CH_4 conversion, 43 % H_2 recovery, and an 81 % reduction in CO_2 emissions. This study underscores the effectiveness of integrating CFD with RSM for the precise modeling and optimization of MRs in BSR reactions. The synergy between these approaches provides a robust framework for advancing the efficiency and sustainability of hydrogen production processes from renewable sources.

1. Introduction

Given the escalating global energy demand and the associated apprehensions regarding finite fossil fuel resources and environmental issues, it is imperative to secure an energy supply in a sustainable manner [1–3]. In response to these challenges, considerable focus has shifted towards hydrogen as a clean and renewable energy carrier. Hydrogen can be produced from either fossil fuels (a conventional practice) or renewable sources. When produced through renewable energy sources and associated to carbon capture, it is often termed "blue hydrogen" [4–6]. Biogas produced from organic wastes via anaerobic digestion may represent a promising renewable feedstock for hydrogen production instead of natural gas. Biogas gaseous mixture mainly consists of methane and carbon dioxide. In addition, it contains a small amount of N_2, H_2, H_2O, H_2S and NH_3 [1,7]. Since 40–80 % of biogas is composed of methane, biogas can be converted into hydrogen through steam reforming (SR), dry reforming (DR), autothermal reforming (ATR) and partial oxidation reforming (POR) processes [8–10].

In particular, due to the presence of CO_2, the DR seems to be the most adequate reforming process for producing hydrogen from a biogas stream. However, the literature shows that, due to the highly

* Corresponding authors.
E-mail addresses: Kamran.ghasemzadeh@manchetser.ac.uk (K. Ghasemzadeh), a.iulianelli@itm.cnr.it (A. Iulianelli).

https://doi.org/10.1016/j.fuel.2024.131205
Received 5 December 2023; Received in revised form 12 January 2024; Accepted 11 February 2024
Available online 17 February 2024

Nomenclature

Acronyms

ANOVA	Analysis of Variance
ATR	Autothermal reforming
BBD	Box-Behnken design
BSR	Biogas steam reforming
CFD	Computational fluid dynamic
DOE	Design of experiments
DR	Dry reforming
GHSV	Gas hour space velocity
MR	Membrane reactor
PBR	Packed bed reactor
RSM	Response surface methodology
SR	Steam reforming
WHSV	Weight hourly space velocity

Symbols

A	Membrane surface (m^2)
$C_{p,i}$	Specific heat capacity of component I (J. Kg^{-1}. K^{-1})
d_p	Catalyst particle diameter (m)
d_i	Inner diameter of the reactor (m)
E_a	Apparent activation energy (KJ•mol^{-1})
J_{H_2}	hydrogen permeating flux (mol•m^{-2}•s^{-1})
M	Molecular weight (kg•mol^{-1})
N_c	Number of components in gas mixture (-)
P	Operating pressure (bar)
$P_{H_{2,ret}}$	Partial pressure for hydrogen in the retentate side (bar)
$P_{H_{2,per}}$	Partial pressure for hydrogen in the permeate side (bar)
q_r	Radial heat flux (J.m^{-2}. s^{-1})
S_i	Source/Sink terms of component i (J•m^{-3}•s^{-1})
T	Operating temperature (K)
V_0	Superficial velocity (m.s^{-1})
$V_{j,i}$	Stoichiometry coefficient of component i in reaction j (-)
y_i	Mole fraction of component i (-)
ε	Porosity of packed bed (-)
μ_i	Dynamic viscosity of component i (kg•m^{-1}•s^{-1})
$\mu_{g.mix}$	Viscosity of the reacting gas mixture (kg•m^{-1}•s^{-1})
ρ_{cat}	Catalyst Density (kg•m^{-3})
ρ_g	Gas Density (kg•m^{-3})
ΔH_j	Heat of reaction j (kJ.mol^{-1})

endothermic nature of this process, significant carbon deposits occur in the reactor during DR in case of operating temperature below those required, leading to catalyst deactivation. On the other hand, biogas steam reforming (BSR), which combines methane DR and SR, can address this problem and increase the hydrogen yield. Therefore, BSR appears to be a more suitable option for hydrogen production from biogas [11]. The catalysts commonly used in SR are transition metals supported on metal oxides. For this process, nickel-based catalysts supported on various matrices, such as SiO_2, Al_2O_3, ZrO_2, etc., are better economical choices compared to noble metals (Pt, Rh, Pd, Ir, etc.) [1,8].

As for the SR of natural gas, conventionally operated in traditional reformers, BSR is an endothermic process, and it is commonly carried out at high temperatures (around 1000 K), in which the thermal radiation affects the endothermic process and products yield significantly [2,12]. However, alternative solutions to the conventional reformers are currently studied to meet the criteria promoted by the Process Intensification Strategy [13], favoring the depletion of the carbon footprint, higher process efficiency and lower costs. In this regard, when applying the concept of membrane reactor (MR) technology to both natural gas SR and BSR, part of the produced hydrogen during the reforming process is removed from the reaction to the permeate side due to the selective hydrogen permeation through a metallic or composite inorganic membrane, collecting a highly concentrated hydrogen stream in the permeate side and shifting the reaction towards the reaction products, meanwhile favoring superior performance in terms of methane conversion and hydrogen yield with respect to the equivalent conventional reformer operated at the same MR conditions [14,15]. In particular, Pd-based membranes represent the dominant membrane solutions to be adopted in MR applications for high grade hydrogen generation and purification due to their exceptional high perm-selectivity towards hydrogen compared to other gases [16].

Although extensive research has been conducted on hydrogen production in Pd-based MRs via methane steam reforming, the number of studies is limited for BSR. However, in recent years, more attention has been focused on this topic. Di Marcoberardino et al. [15] found that MRs offered improved efficiency and economics over conventional reactors for BSR to produce green hydrogen. Castillo et al. [17] achieved 50–80 % hydrogen recovery in a Pd-Ag MR at 623–723 K versus a conventional reactor approaching equilibrium, while Iulianelli et al. [10] faced challenges in a self-supported Pd-Ag membrane degradation by H_2S contained in a synthetic biogas feed stream carrying out BSR in a MR, reaching methane conversion $\geq$ 80 %, and hydrogen purity > 99.999 %, operating at 623 K and 2 bar. Parente et al. [18] demonstrated that, despite temperature limitations, Pd-MRs yielded high-purity hydrogen from BSR, offering a cleaner and renewable pathway for hydrogen production at lower temperatures than conventional reactors.

However, most of the studies conducted on the BSR process in MRs are experimental works. There has been less emphasis on the numerical simulation methods, which can provide valuable insights into this process in a cost-effective manner. CFD is a valuable technique that employs numerical methods to estimate the governing equations of fluid mechanic within a specified domain [19]. There is a number of studies in which CFD analyses have been conducted to investigate theoretically the CO_2 methanation [20,21] and hydrogen production from methane SR and DR reforming [22,23], methanol SR [24], water gas shift [25], glycerol SR [26] and biomass gasification [27] in MRs. Regarding the BSR process, several modeling studies have been reported in literature. Cipiti et al. [28] developed a model of a BSR reactor including mass/heat transport and kinetics to simulate the process and optimize parameters. The Comparison between the model and experimental data indicated that the model accurately predicted product distribution and reactor performance for advancing fuel reforming technology. Hajjaji et al. [29] performed a life cycle assessment of a BSR system for hydrogen production using Aspen plus. BSR achieved about half the greenhouse gas emissions of conventional SR of methane. The assessment showed how biogas was an eco-friendly and sustainable source for hydrogen production. Rosa et al. [30] developed a model to identify optimal conditions for mixed reforming of biogas to produce hydrogen. With biogas composed of 50–60 % CH_4, the results indicated that the ideal conditions, at temperatures between 1008 and 1063 K, can yield hydrogen as efficiently as pure methane.

In the case of BSR process in MRs, CFD can simulate detailed gas flow characteristics at any point in the reactor, providing insights for virtual prototyping [27]. A recent theoretical study about BSR reaction carried out in Pd-MRs for hydrogen production was proposed by Caldas et al. [31] where 2D non-isothermal models were developed at laboratory and industrial scales. The findings suggested an optimal temperature range (823–948 K) for achieving a balance between reaction performance and hydrogen permeation rate. Lower velocities of 0.046 m/s gave better performance, providing key data to optimize and design membrane modules. This modeling study demonstrated BSR's feasibility in MRs and provided design insights.

The performance and efficiency of hydrogen production from biogas in a MR are influenced by numerous design and operational factors as well as hydrodynamic parameters. Therefore, it is essential to identify the optimal conditions of variables and their interactions. In this regard, response surface methodology (RSM) is an accurate, useful, and cost-effective tool for predicting the relationship between input and output parameters [32–35]. RSM represents an effective and widely employed statistical approach for optimizing and predicting processes that involve multiple variables. One of its primary advantages is the ability of efficiently analyzing and optimizing complex systems, meanwhile requiring a few experimental runs instead of a complete experimental design. This not only enhances the effectiveness of the study but also conserves valuable time and resources.

Integrating optimization methodologies like RSM with numerical models prevents expensive and time-intensive experiments, meanwhile enabling the determination of optimal conditions using different input combinations [32,35]. However, there is a notable gap in parametric analysis and optimization of Pd-Ag MR performance during BSR process. To the best of our knowledge, there are no studies implementing the CFD modeling with RSM methodology to analyze theoretically BSR reaction in MRs. Therefore, in this work it was developed a novel comprehensive CFD-RSM model to simulate the BSR in a Pd-Ag MR in order to conduct a parametric study on key operating parameters including temperature, pressure, GHSV, feed ratio, and sweep gas ratio. The impacts on hydrogen recovery and purity, methane conversion and carbon dioxide emission reduction has been analyzed in detail. Last but not least, an optimization study of BSR process by integrating RSM analysis has been performed to determine the optimum among the analyzed operating conditions to get the best performance in the MR system.

2. CFD model development

In this study, a 2D-axisymmetric model was developed using COMSOL Multiphysics 6.1 software to investigate the performance of the BSR process in a Pd-Ag MR. Furthermore, RSM analysis was employed to assess the impact of operational parameters on response variables and identify optimal conditions.

The main assumptions are:

1) steady-state conditions;
2) full hydrogen perm-selectivity of the dense Pd-Ag membrane with respect to all of the other gases;
3) the reaction occurs only at the catalyst surface; hence, there is no mass transfer resistance between the bulk gas and the catalyst surface;
4) physical properties, such as gas density, are constant with the temperature;
5) the film transport resistance supposed at the interface of gas/membrane was considered negligible;
6) mechanical stability of Pd-Ag membrane at lower temperatures;
7) pseudo-homogenous condition in reaction zone.

2.1. Modeling configuration and meshing

In this study, the experimental setup utilized in our previous publication [6] was adopted to configure the Pd-Ag MR. The MR module geometrical characteristics include an internal diameter of 0.02 m and a length of 0.2 m. It houses a self-supported tubular Pd-Ag membrane with an external diameter of 0.01 m, and a length of 0.145 m, as schematized in Fig. 1.

To assess its performance, this MR was compared with respect to a geometrically equivalent conventional packed bed reactor (PBR) under identical operating conditions. The characteristics of the MR and PBR setups are summarized in Table 1.

Some experimental data obtained in the experimental campaign carried out in our previous study [6] were used to validate the CFD model simulating the behavior of a Pd-Ag MR packed with 3 g of Ni-based catalyst to produce high grade hydrogen via BSR reaction. The model's computational domain was divided into a structured grid using meshes.

To obtain the optimal number of mesh grids, mesh independency analysis was conducted in Section 2.4. This is because, although increasing the number of meshes improves prediction results in terms of accuracy, it also leads to increased computational costs and time.

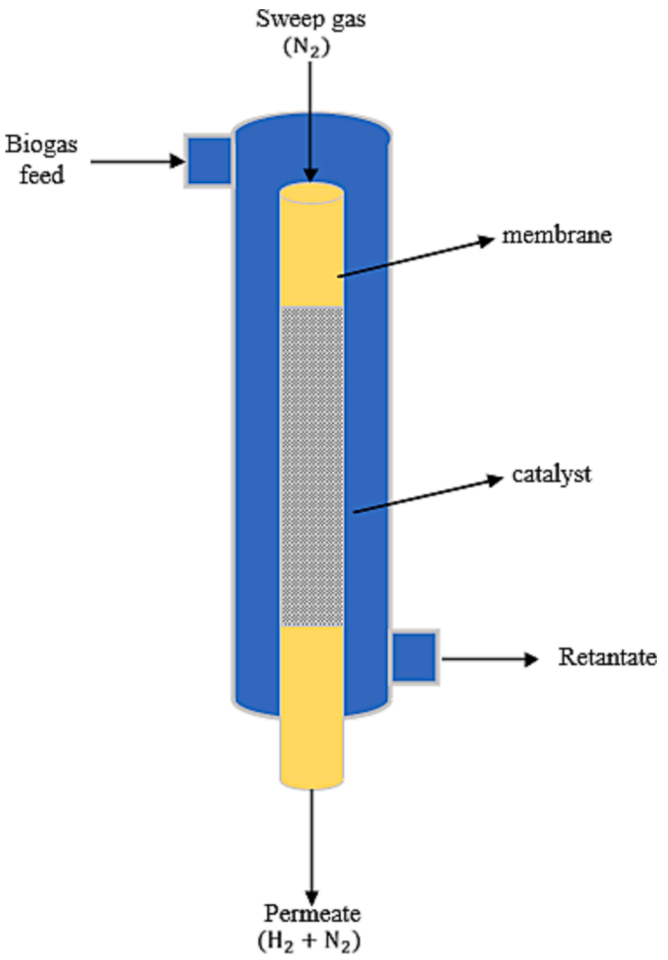

Fig. 1. Simulated Pd-Ag MR schemes for the process of biogas steam reforming.

Table 1
Characteristics of the MR and packed bed reactor setups.

Parameter	Membrane reactor	Packed bed reactor
Reactor height (m)	0.145	0.145
Outer diameter of the reactor (m)	0.03	0.03
Inner diameter of the reactor (m)	0.02	0.01
Membrane length (m)	0.145	–
Membrane thickness (m)	150×10^{-6}	–
Outer diameter of membrane (m)	0.01	–
Catalyst	Cylindrical shape Ni-based	Cylindrical shape Ni-based

2.2. Kinetic model

The kinetic equations proposed by Xu and Froment [36] for methane SR, which are widely accepted as the most accurate kinetic model for

this reaction, were utilized in our CFD model to describe the BSR kinetic mechanism. The chemical reactions considered for the BSR reaction include:

Steam reforming of methane.

$$CH_4 + H_2O \rightarrow CO + 3H_2 \Delta H_r^0 = 206.1\ kJ/mol \quad (1)$$

Water gas shift reaction

$$CO + H_2O \rightarrow CO_2 + H_2 \Delta H_r^0 = -41.2\ kJ/mol \quad (2)$$

Reverse methanation reaction

$$CH_4 + 2H_2O \rightarrow CO_2 + 4H_2 \Delta H_r^0 = 206.1\ kJ/mol \quad (3)$$

The rate of the three reactions (Eqs.1–3) are calculated through the following expressions:

$$r_1 = \frac{k_1}{P_{H_2}^{2.5}}\left(P_{CH_4}P_{H_2O} - \frac{P_{H_2}^3 P_{CO}}{K_{eq_1}}\right)/DEN^2 \quad (4)$$

$$r_2 = \frac{k_2}{P_{H_2}}\left(P_{CO}P_{H_2O} - \frac{P_{H_2}P_{CO_2}}{K_{eq_2}}\right)/DEN^2 \quad (5)$$

$$r_3 = \frac{k_3}{P_{H_2}^{3.5}}\left(P_{CH_4}P_{H_2O}^2 - \frac{P_{H_2}^4 P_{CO_2}}{K_{eq_3}}\right)/DEN^2 \quad (6)$$

$$DEN = 1 + K_{CH_4}P_{CH_4} + K_{CO}P_{CO} + K_{H_2}P_{H_2} + \frac{K_{H_2O}P_{H_2O}}{P_{H_2}} \quad (7)$$

The equilibrium, kinetics and adsorption constants, which were used in the reaction rates equations, are calculated as reported in Table 2.

2.3. Governing equations

To develop an accurate CFD model, it is crucial to solve the following differential equations: mass balance to track molar changes, momentum balance to determine pressure along the reactor length, and energy balance to calculate temperature changes.

2.3.1. Mass balance

Mass balance equations, which are used to compute the molar changes of different component including CH_4, H_2O, CO, H_2, and CO_2 along the reactors, are expressed as follows:

$$\frac{dN_i}{dz} = \rho_{cat}(1-\varepsilon)\sum_{j=1}^{3}\eta_j \nu_{j,i} r_j + S_i \quad (8)$$

where, N is the molar flux, subscripts i and j represent i^{th} component and j^{th} reaction number (Eqs.1–3), respectively, ε is porosity of packed bed and ρ is catalyst density. η_j and r_j are the effectiveness factor and rate of reaction j, respectively. $\nu_{j,i}$ is the stoichiometric coefficient of component i in reaction j.

S_i is the sink/source terms of component i, which accounts the permeating flux of each i-component through the membrane. Here, since the membrane is fully hydrogen perm-selective, this term is only applied for hydrogen mass balance and calculated as:

$$S_i = \frac{A J_{H_2}}{V} \quad (9)$$

A is the membrane surface, V the computational cell volume, and J_{H_2} is the hydrogen permeating flux, calculated by Sieverts-Fick law:

$$J_{H_2} = Pe_{H_2}^0 \exp\left(\frac{-E_a}{RT}\right)\left(p_{H_2,ret}^{0.5} - p_{H_2,per}^{0.5}\right) \quad (10)$$

$Pe_{H_2}^0$, E_a, $p_{H_2,ret}$ and $p_{H_2,per}$ are a constant coefficient, the apparent activation energy, and hydrogen partial pressure in the retentate and permeate sides, respectively.

2.3.1.1. Momentum equations for gas phase. The Ergun equation is a commonly used momentum equation for determining the pressure drop in packed bed reactors. This equation is expressed as:

$$\frac{dP}{dz} = \frac{150\, V_0\, \mu_{g,mix}}{d_p^2}\frac{(1-\varepsilon)^2}{\varepsilon^3} + \frac{1.75\, \rho_g\, V_0^2}{d_p}\frac{1-\varepsilon}{\varepsilon^3} \quad (11)$$

In this equation, the first term accounts the viscous loss, which is dominant in laminar flow, and the second term accounts the kinetic-energy losses, which are dominant in high Reynolds numbers, and are caused mainly by changes in shape and direction of channels among the particles.

In the Ergun equation, the parameters are defined as follows: d_p is the catalyst particle diameter, V_0 is the superficial velocity, ε is the bed porosity, ρ_g is the gas density, and $\mu_{g,mix}$ is the viscosity of the reacting gas mixture. Gas viscosity ($\mu_{g,mix}$) is calculated using the following equation:

$$\mu_{g,mix} = \sum_{i=1}^{N_C}\frac{y_i\mu_i}{\sum_{j=1}^{N_c} y_i\left(\frac{M_i}{M_i}\right)^{0.5}}, \quad \frac{kg}{m\,s} \quad (12)$$

where, y_i, μ_i are the mole fraction and viscosity of i^{th} component, and M and N_c are the molecular weight and number of components in gas mixture, respectively. The viscosity of each component is calculated using the following equation:

$$\mu_i = \frac{AT^B}{1 + \frac{C}{T} + \frac{D}{T^2}}, \quad \frac{kg}{m\,s} \quad (13)$$

The A, B, C and D constant values can be found in [11].

2.3.2. Heat transfer equation for gas phase

The energy balance for the modeled MR is given by:

$$\frac{dT}{dz} = \frac{\rho(1-\varepsilon)\left(\sum_{j=1}^{3} -\Delta H_j r_j \eta_j\right) + \frac{4\, q_r}{d_i} + S_{H_2} C_{p,H_2} T}{\sum_{i=1}^{5} N_i C_{p,i}} \quad (14)$$

where ΔH_j, $C_{p,i}$, q_r and d_i are the heat of reaction j, specific heat capacity of component i, radial heat flux, and inner diameter of the reactor,

Table 2
Kinetic parameters for BSR [11].

Category	Parameters	Units
Kinetic rate constants	$k_1 = 9.49 \times 10^{15}\exp\left(\frac{-240100}{RT}\right)$ $k_2 = 4.39 \times 10^{6}\exp\left(\frac{-67130}{RT}\right)$ $k_3 = 2.29 \times 10^{15}\exp\left(\frac{-243900}{RT}\right)$	$\frac{kmol.bar^{0.5}}{kg_{cat}hr}$ $\frac{kmol.bar^{-1}}{kg_{cat}hr}$ $\frac{kmol.bar^{0.5}}{kg_{cat}hr}$
Equilibrium constants	$K_{eq_1} = \exp\left(\frac{-26830}{T} + 30.114\right)$ $K_{eq_2} = \exp\left(\frac{4400}{T} - 4.063\right)$ $K_{eq_3} = K_{eq_1} \times K_{eq_2}$	bar^2(-) bar^2
Adsorption constants	$K_{CH_4} = 6.65 \times 10^{-4}\exp\left(\frac{38280}{RT}\right)$ $K_{H_2O} = 1.77 \times 10^{5}\exp\left(\frac{-88680}{RT}\right)$ $K_{CO} = 8.23 \times 10^{-5}\exp\left(\frac{70650}{RT}\right)$ $K_{H_2} = 6.12 \times 10^{-9}\exp\left(\frac{82900}{RT}\right)$	bar^{-1}(-) $bar^{-1}bar^{-1}bar^{-1}$

respectively.

2.3.3. Boundary conditions and post processing definitions

Boundary conditions employed in the CFD simulations of the Pd-Ag MR, for both the permeate and retentate sides, are summarized in Table 3.

The following equations are the main parameters useful to describe the performance of the Pd-Ag MR during the BSR reaction:

$$\text{Methane conversion}\ (\%) = \frac{CH_{4,in} - CH_{4,out}}{CH_{4,in}} \times 100 \quad (15)$$

$$CO_2\ \text{emission reduction}\ (\%) = \frac{CO_{2,in} - CO_{2,out}}{CO_{2,in}} \times 100 \quad (16)$$

$$\text{Hydrogen recovery}(\%) = \frac{H_{2,perm}}{H_{2,perm} + H_{2,ret}} \times 100 \quad (17)$$

where $CH_{4,in}$, $CH_{4,out}$, $CO_{2,in}$ and $CO_{2,out}$ represent the inlet and outlet methane and carbon dioxide molar flow rates, respectively. Additionally, $H_{2,perm}$ and $H_{2,ret}$ are the moles of hydrogen permeated through the membrane and the moles of hydrogen on the retentate side, respectively.

Numerical procedure and mesh independency

The CFD model's governing equations were solved utilizing the finite-element method, and corrections to pressure–velocity were carried out employing the Semi-Implicit Method for Pressure Linked Equations (SIMPLE) algorithm. The computational model integrates standard definitions for fluid and heat properties, considering their dependencies on temperature, pressure, and composition. The numerical solution persisted until the tolerance value for all variables was less than 10^{-4}. To ensure that simulation results were independent of mesh size, preliminary tests were conducted under the following operating conditions: reaction pressure of 350 kPa, reaction temperature of 673 K, H_2O/CH_4 ratio of 2/1, and WHSV of 0.2 h^{-1}.

These tests focused on methane conversion in both MR and PBR, using different mesh numbers: 2056, 4019, 8036, 10972, 20467, and 40129. As shown in Fig. 2, the results indicate that there are no significant differences in methane conversion between mesh numbers 10972, 20467, and 40,129 for both MR and PBR. Therefore, a mesh number of 10,972 is considered the optimal choice for subsequent simulations.

2.4. Model validation

To rely on CFD model results accuracy, the CFD model was validated experimentally. To this aim, the theoretical results were compared with experimental data obtained in our previous work [6] (see Fig. 3).

The systems and operating conditions were identical in both the CFD simulations of the MR and PBR operations, and specifically carried out at 673 K, $H_2O/CH_4 = 2/1$ and with a WHSV of 0.2 h^{-1}. The comparison results indicated a minimum relative error of 1 % and a maximum relative error of 9.6 %, which have been considered acceptable within the context of this study. This direct comparison of CFD predictions and experimental measurements validated the accuracy of the CFD model under these conditions.

Table 3
Boundary conditions set for the CFD simulations of retentate and permeate sides of the Pd-Ag membrane reactor.

Position	Flow rate for retentate side	Flow rate for permeate side
Inlet (Z = 0)	CH_4 molar flow rate	–
Inlet (Z = 0)	H_2O molar flow rate	Sweep gas flow rate
Inlet (Z = 0)	CO_2 molar flow rate	–
Inlet (Z = 0)	Feed pressure	Sweep gas pressure
Outlet (Z = L)	Outlet pressure	Outlet pressure

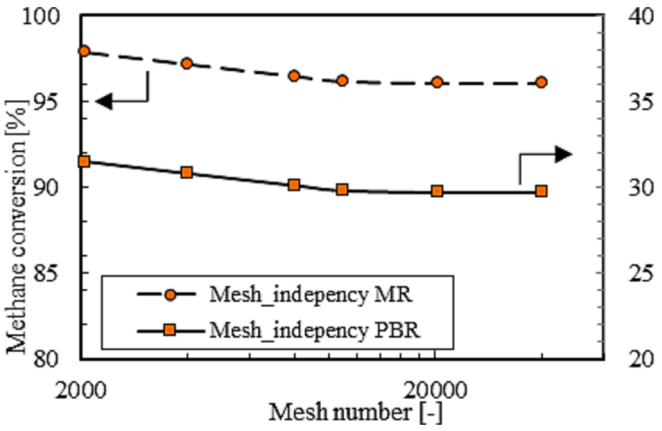

Fig. 2. Effect of mesh numbers on calculated methane conversion by CFD model for the case of the MR and PBR at a reaction pressure of 350 kPa, reaction temperature of 673 K, WHSV of 0.2 hr^{-1} and H_2O/CH_4 of 2/1.

3. Experimental design procedure

The design of experiments (DOE) using RSM combined with a Box-Behnken Design (BBD) was implemented using Design-Expert v13.1.2 software to systematically analyze and optimize the BSR process in the Pd-Ag MR. This allowed efficient examination of the effects of individual factors as well as factor interactions with fewer trials compared with other DOE methods [33]. The input parameters studied were reaction temperature, pressure, gas hourly space velocity (GHSV), H_2O/CH_4 molar ratio, and sweep gas/feed molar ratio (S/F). The response factors focused on CH_4 conversion, H_2 recovery, and CO_2 emission reduction. According to the BBD matrix, a total of 41 simulations were conducted in COMSOL Multiphysics employing the customized CFD model, with the factors configured at various combinations of levels, as detailed in Table 4. The CFD simulation results for CH_4 conversion, H_2 recovery, and CO_2 emission reduction for each run were used as input data to the Design-Expert to generate response surface quadratic models correlating the factors and responses. The RSM method used in this study included second-order polynomial models for indicating the relationships between input parameters and output responses. Eq. (23) represents the general form of these models [34]:

$$Y = \beta_0 + \sum_{i=1}^{5} \beta_i X_i + \sum_{i=1}^{5} \beta_{ii} X_{ii}^2 + \sum_{i=1,j=1}^{5} \beta_{ij} X_i X_j \quad (23)$$

where Y is the response factor (CH_4 conversion, H_2 recovery and CO_2 emission reduction), while X shows input variables that can be A: Reaction temperature, B: Reaction pressure, C: GHSV, D: H_2O/CH_4 and E: S/F, β_0 is the constant coefficient, β_i and β_{ii} and β_{ij} are linear effect, square and interactive terms, respectively. Analysis of variance (ANOVA) was performed to determine the interactions between the independent process parameters and the response variables. The quality of the model was evaluated using the coefficient of determination R^2_{adj} and R^2. The statistical significance was assessed by F-values, p-values, and adequate precision ratio. ANOVA enabled quantification of the effects of the independent variables and their interactions on the response [32].

4. Results and discussion

4.1. Statistical analysis

Regarding the process optimization, a five-factor and three-level Box-Behnken method was used to evaluate the relative importance of the selected factors for CH_4 conversion, H_2 recovery, and CO_2 emission reduction through CFD simulations, as detailed in Table 5. ANOVA was

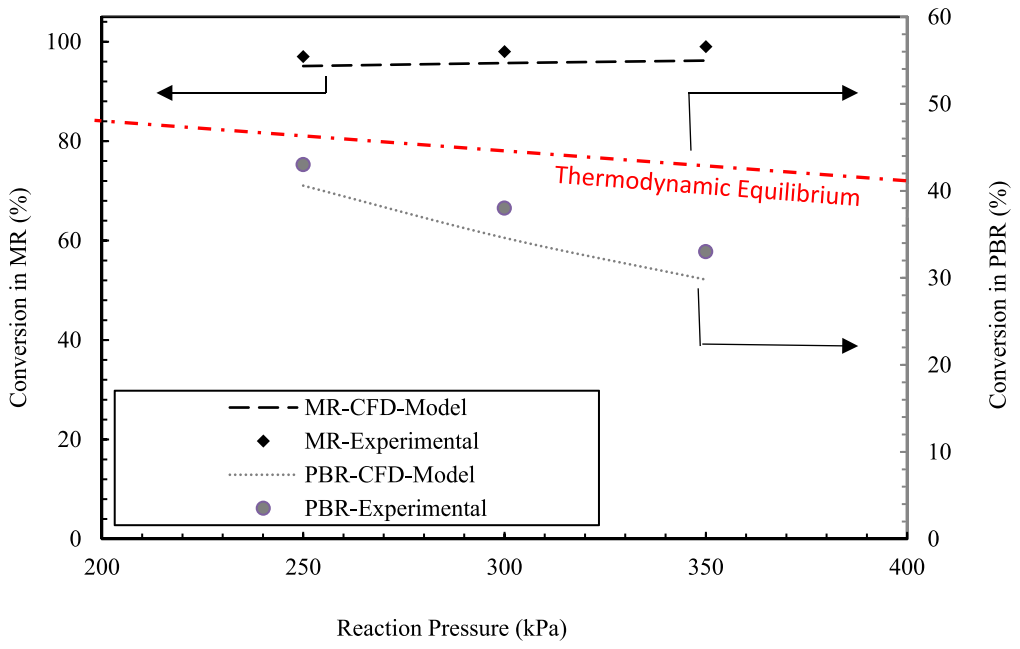

Fig. 3. Comparison of CH_4 conversion in MR and in PBR with experimental data from literature at 673 K and S/C = 2/1 [6].

Table 4
Coded levels of five input variables and Box Behnken design matrix.

Run N.	A: Reaction temperature (K)	B: Reaction pressure (bar)	C: GHSV (h^{-1})	D: H_2O/CH_4 (-)	E: S/F (-)
1	643	4	9000	1	9
2	603	4	9000	3	5
3	643	4	15,000	3	5
4	643	4	3000	2	9
5	643	4	9000	3	9
6	603	4	3000	2	5
7	683	4	3000	2	5
8	643	2	9000	1	5
9	603	4	9000	2	9
10	643	6	3000	2	5
11	643	4	15,000	2	9
12	643	4	3000	3	5
13	603	4	15,000	2	5
14	643	4	9000	2	5
15	643	2	9000	3	5
16	683	4	9000	2	1
17	643	6	9000	2	9
18	643	4	3000	2	1
19	643	4	9000	1	1
20	603	4	9000	1	5
21	643	2	9000	2	1
22	603	4	9000	2	1
23	643	4	15,000	1	5
24	603	2	9000	2	5
25	683	4	9000	3	5
26	683	4	9000	2	9
27	643	6	9000	3	5
28	643	4	15,000	2	1
29	683	4	15,000	2	5
30	683	6	9000	2	5
31	643	4	3000	1	5
32	643	4	9000	3	1
33	683	4	9000	1	5
34	643	6	15,000	2	5
35	643	2	15,000	2	5
36	643	2	9000	2	9
37	643	2	3000	2	5
38	643	6	9000	2	1
39	643	6	9000	1	5
40	683	2	9000	2	5
41	603	6	9000	2	5

conducted to statistically assess the developed model, and the results obtained from the simulations have been fitted to second-order polynomial equations to establish the relationship between the factors and responses of the regression equations for CH_4 conversion (Y_1), H_2 recovery (Y_2) and CO_2 emission reduction (Y_3) in terms of factor coded values, as presented by Eqs. (24)–(26):

$$Y_1 = 39 + 24.84A + 6.37B - 11.97C + 8.38D + 4.38E + 2.25AB - 4.38AC + 2AD + 1.25AE - 1.5BC + 1.5BD + 0.25BE - 1.25CD - 0.25CE + 0.25DE + 7.30A^2 - 0.3229B^2 + 6.30C^2 - 0.1562D^2 - 0.6563E^2 \quad (24)$$

$$Y_2 = 21 + 9.88A + 3.13B - 4.44C - 1.62D + 1.94E + AB - 1.25AC - 0.25AE - BD - 1.5BE + 0.25CD - 0.25CE - 0.25DE + 1.1A^2 - 1.4B^2 + 0.8542C^2 - 0.2292D^2 - 0.6458E^2 \quad (25)$$

$$Y_3 = 20 + 22.37A + 5.44B - 8C + 15.5D + 3.06E + 3.25AB - 3.25AC + 1.5AD + 1.5AE - BC - 0.75BD + 0.75BE + 3CD - 1.25CE + 1.75DE + 10.75A^2 + 2.33B^2 + 8.42C^2 + 3.08D^2 - 1.33E^2 \quad (26)$$

The coefficient values in Eqs. (24)–(26) indicate the influence of each parameter (A: reaction temperature, B: reaction pressure, C: GHSV, D: CH_4/H_2O and E: S/F) and their interactions on the responses. Positive coefficient values increase the response magnitude, while negative values decrease the response measure. Regression coefficients and p-values are provided in Table 5, where p-values less than 0.05 indicate a significant impact of the term on the response. Terms with p-values greater than 0.05 do not significantly affect the model's prediction accuracy and can be deleted from the model equation [33]. According to the ANOVA results presented in Table 6, the F-values (252.74, 61.26 and 19.56) and p-values < 0.0001 for all three responses indicate that the models provided for the investigated inputs variable range are suitable for representing hydrogen production in the Pd-Ag MR.

The coefficient of determination (R^2) from the ANOVA statistical output indicates the level of correlation between input parameters and response variables. Values closer to 1 indicate a stronger correlation and better model fit. The R^2 values for CH_4 conversion, H_2 recovery, and CO_2

Table 5
Regression Coefficients and P-Values of the RSM models.

Model Terms	CH_4 Conversion Coefficient	p-values	H_2 Recovery Coefficient	p-values	CO_2 Emission reduction Coefficient	p-values
Intercept	39		21		20	
A (Reaction temperature)	24.8438	< 0.0001	9.875	< 0.0001	22.375	< 0.0001
B (Reaction pressure)	6.375	< 0.0001	3.125	< 0.0001	5.4375	0.0021
C (GHSV)	−11.9688	< 0.0001	−4.4375	< 0.0001	−8	< 0.0001
D (H_2O/CH_4)	8.375	< 0.0001	−1.625	< 0.0001	15.5	< 0.0001
E (S/F)	4.375	< 0.0001	1.9375	< 0.0001	3.0625	0.061
AB	2.25	0.0172	1	0.1521	3.25	0.3047
AC	−4.375	< 0.0001	−1.25	0.0775	−3.25	0.3047
AD	2	0.0317	3.76E-18	1	1.5	0.6321
AE	1.25	0.1644	−0.25	0.7136	1.5	0.6321
BC	−1.5	0.0987	−5.32E-17	1	−1	0.7492
BD	1.5	0.0987	−1	0.1521	−0.75	0.8104
BE	0.25	0.7758	−1.5	0.0371	0.75	0.8104
CD	−1.25	0.1644	0.25	0.7136	3	0.3424
CE	−0.25	0.7758	−0.25	0.7136	−1.25	0.6896
DE	0.25	0.7758	−0.25	0.7136	1.75	0.5768
A^2	7.30208	< 0.0001	1.10417	0.1635	10.75	0.0061
B^2	−0.322917	0.7463	−1.39583	0.0824	2.33333	0.5133
C^2	6.30208	< 0.0001	0.854167	0.2764	8.41667	0.0262
D^2	−0.15625	0.8755	−0.229167	0.7671	3.08333	0.3896
E^2	−0.65625	0.5126	−0.645833	0.4075	−1.33333	0.7077

Table 6
The ANOVA output for response surface quadratic models of CH_4 conversion, H_2 recovery and CO_2 emission reduction.

Response	Sum of squares	df	Mean square	F-value	P-Value	R^2	Adjusted R^2	Adequate precision
CH_4 conversion	15164.51	20	758.23	252.74	< 0.0001	0.9961	0.9921	63.6215
H_2 recovery	2210.31	20	110.52	61.26	< 0.0001	0.9839	0.9679	31.0129
CO_2 emission reduction	14891.49	20	744.57	19.56	< 0.0001	0.9514	0.9027	17.1555

emission reduction were equal to 0.9961, 0.9839, and 0.9514, respectively. The high R^2 values demonstrate a suitable alignment of the response models with CFD simulations. Additionally, an adequate precision, which measures signal-to-noise ratio and, when greater than 4, indicates an effective model, was found to be equal to 63.6215, 31.0129, and 17.1555 for these cases. Therefore, the model is suited for navigation of the design space.

4.2. Effect evaluation of operating parameters

4.2.1. Evaluation of reaction temperature effect

Methane is converted through reactions that are highly endothermic. Hence, an increase of temperature rises both the reaction rates and the available equilibrium conversions. Therefore, as shown in Fig. 4a, higher temperatures lead to higher CH_4 conversions. Additionally, the Arrhenius-like temperature dependence of hydrogen permeation leads to increased hydrogen permeation fluxes at higher temperatures. Fig. 4b illustrates that, since higher hydrogen permeation fluxes favour a greater removal of hydrogen from the reaction side towards the permeate side of the MR, this is responsible for the shift effect of the reactions involved during BSR towards the products, due to the Le Chatelier's principle. Consequently, this is the reason why this mechanism involves higher H_2 recoveries and CH_4 conversions. The obtained results (Fig. 4c) show that an increase of temperature leads to an increase in the CO_2 emission reduction value. This result describes indirectly how the effect of temperature on the DR of CH_4 (Eq. (4) is significant and how this reaction presents the highest temperature sensibility.

4.2.2. Evaluation of reaction pressure effect

In the key reaction of the proposed scheme, such as the SR of CH_4, it is observed that the number of moles of the products is higher than the moles number of the reactants. Consequently, from a thermodynamic point of view, an increase of pressure suppresses the forward reactions and reduces CH_4 conversion. However, Fig. 5a shows that a higher pressure enhances CH_4 conversion. This is due to a second opposed effect of pressure on CH_4 conversion. As derived from Eq. (10), higher pressure improves the driving force of the hydrogen permeation through the membrane.

Hence, the higher the pressure the higher the hydrogen permeation driving force and the removal of hydrogen from the reaction zone to the permeate side is consequently larger, shifting the SR of CH_4 towards higher CH_4 conversions. The simulations proposed in Fig. 5a point out that the shift effect dominates over the competing thermodynamic effect when the pressure raises, involving a progressive increase in CH_4 conversion. In particular, increasing pressure from 2 to 6 bar raises CH_4 conversion about 10 %.

Furthermore, in addition to its impact on CH_4 conversion, the higher permeation fluxes determined by exercising the MR at higher pressures improve the hydrogen recovery (Fig. 5b). However, the proposed simulations showed that the theoretical performance of the MR exercised under BSR reaction were not exceptional as the reaction temperature set for the MR was much below the required temperature in the equivalent conventional reactor.

4.2.3. Evaluation of GHSV effect

GHSV is inversely related to the residence time. Therefore, a GHSV increase leads to lower contact time for reaction reactants and lower CH_4

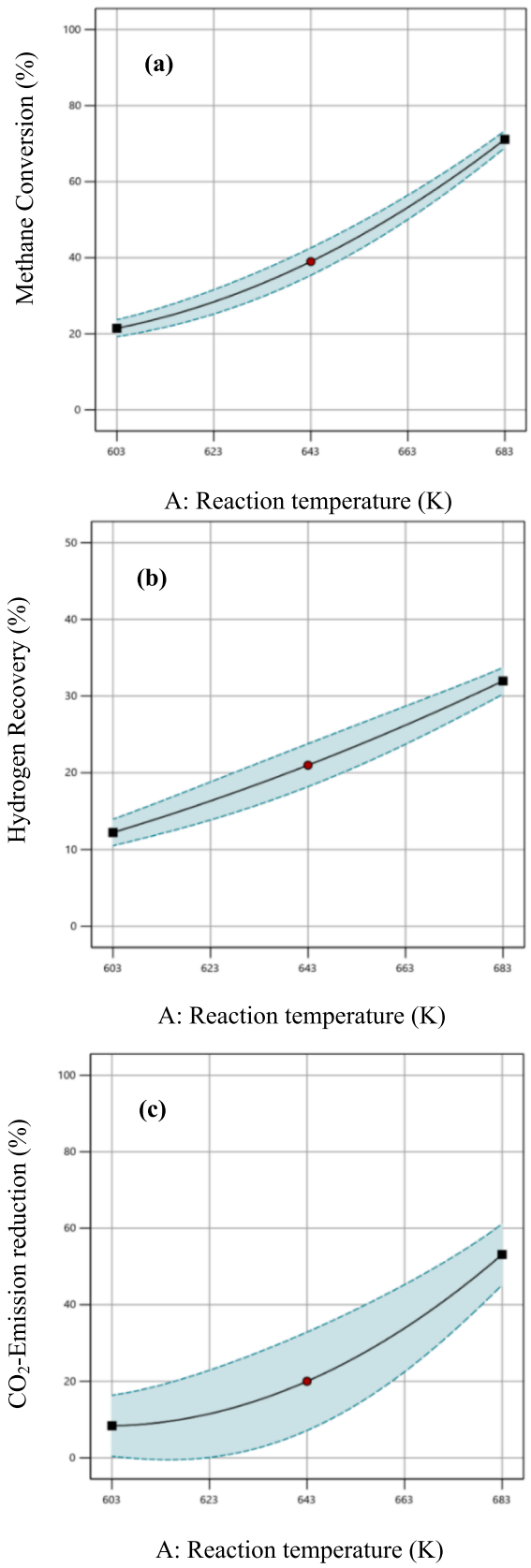

Fig. 4. a) CH_4 conversion, b) H_2 recovery, and c) CO_2 emission reduction versus reaction temperature (K) at reaction pressure = 4 bar, GHSV = 9000 h^{-1}, H_2O/CH_4 = 2 and S/F = 5.

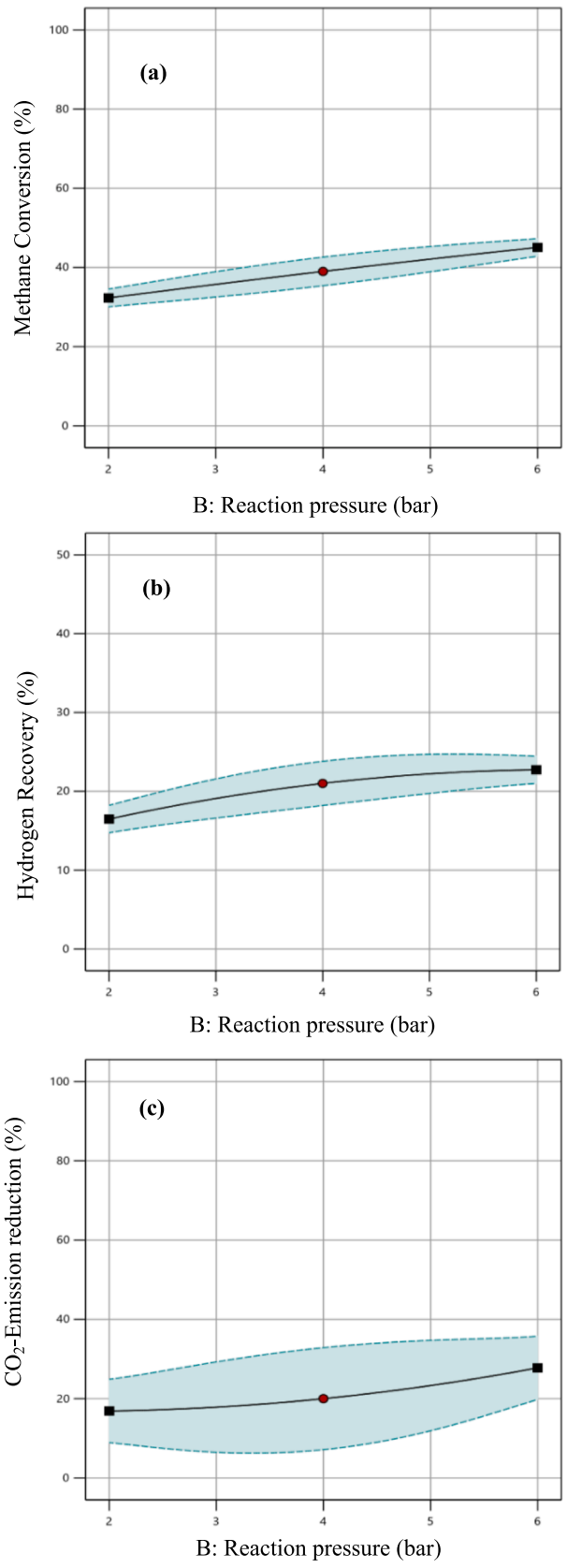

Fig. 5. A) ch_4 conversion, b) H_2 recovery, and c) CO_2 emission reduction versus reaction pressure at reaction temperature = 673 K, GHSV = 9000 h^{-1}, H_2O/CH_4 = 2 and S/F = 5.

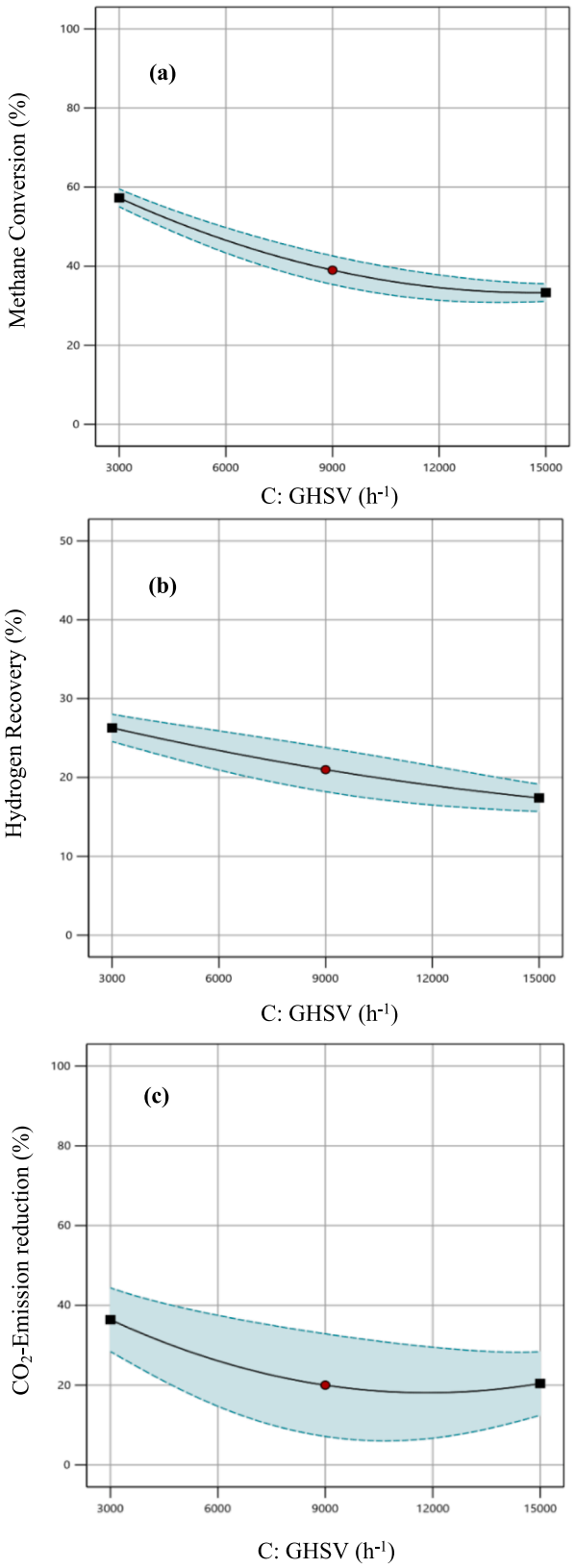

Fig. 6. A) ch_4 conversion, b) H_2 recovery, and c) CO_2 emission reduction versus GHSV value (at reaction pressure = 4 bar, reaction temperature = 673 K, H_2O/CH_4 = 2 and S/F = 5).

conversions. Fig. 6a shows that, when GHSV becomes 5 times larger, it increases from 3000 to15000 h^{-1}, and the CH_4 conversion reduces about 20 %. In Fig. 6b, the simulations highlight that higher flow rates promote faster transit of components through the MR reaction side, reducing the percentage of hydrogen that can permeate through the Pd-Ag membrane, lowering the hydrogen removal, the shift effect on the reaction system and the hydrogen recovery as well. The decrease in both hydrogen recovery and CH_4 conversion reduces the performance of the MR in terms of CO_2 emission reduction (Fig. 6c).

4.2.4. *Evaluation of feed molar ratio (H_2O/CH_4) effect*

As shown in Fig. 7a, a higher feed molar ratio leads to higher CH_4 conversion. Thus, the presence of a larger steam content in the reaction zone favorably affects catalyst activity and promotes the reactions towards higher CH_4 consumption and hydrogen production. However, Fig. 7b shows also that a higher feed molar ratio reduces hydrogen recovery due to the dilution effect of the water presence on the retentate side. This is responsible for the reduction of the hydrogen partial pressure in this side and consequently the hydrogen permeation driving force, depleting the hydrogen permeating flux and the hydrogen recovery as well. Therefore, an optimal feed molar ratio is needed to balance the different effects of this parameter on CH_4 conversion and hydrogen recovery. As described, the feed molar ratio improves reactor activity but undesirably affects the hydrogen permeation. Better reaction zone performance means more effective BSR performance and greater reduction in CO_2 emissions (Fig. 7c).

4.2.5. *Evaluation of sweep gas ratio effect*

Sweep gas is used on the permeate side to sweep away the permeated hydrogen, reducing its partial pressure in this side and consequently improving the hydrogen permeation driving force, leading to better performance in terms of CH_4 conversion, hydrogen recovery and CO_2 emission reduction, Fig. 8. An increase of the sweep gas ratio up to 9 times results in a hydrogen recovery improvement of less than 5 % and a CO_2 emission reduction of less than 2 %. Therefore, higher sweep gas ratios are not recommended.

4.3. *Evaluation of component/velocity distribution*

Fig. 9 illustrates the axial concentration contours for the components present in a Pd-Ag MR during the BSR process carried out at 673 K, 4 bar, H_2O/CH_4 = 2 and S/F = 5. The figure illustrates the evolution of CH_4, H_2O, CO_2, and H_2 concentrations along the reactor's length. With the inlet of biogas and H_2O into the MR's catalytic bed, the BSR reaction takes place, resulting in decreasing CH_4 and H_2O concentrations along the reactor. CO_2 concentrations initially decrease due to consumption through DR (Eq. (4), but subsequently increase due to simultaneous production by the reaction represented in Eq. (3).

Simultaneously with the production of H_2, it permeates through the full hydrogen perm-selective Pd-Ag membrane, with its concentration increasing along the permeate side.

The pressure distribution on the permeate and retentate sides of the MR is depicted by the colored contours in Fig. 10. The pressure drops on the permeate side is approximately 0.02 bar, and on the retentate side, due to the presence of the catalytic bed, is around 0.06 bar.

4.4. *Optimization and sensitivity analysis*

The CFD model combined with statistical approach of Box-Behnken was used for determining the optimal values of input parameters to achieve maximum CH_4 conversion, H_2 recovery and CO_2 emission reduction in the proposed Pd-Ag MR. Optimization is an essential tool for extensive design, modeling, and implementation of large-scale processes. It is a mathematical approach used to systematically identify the optimal values from a given input dataset by selecting independent variables within predefined limits and predicting the optimal response.

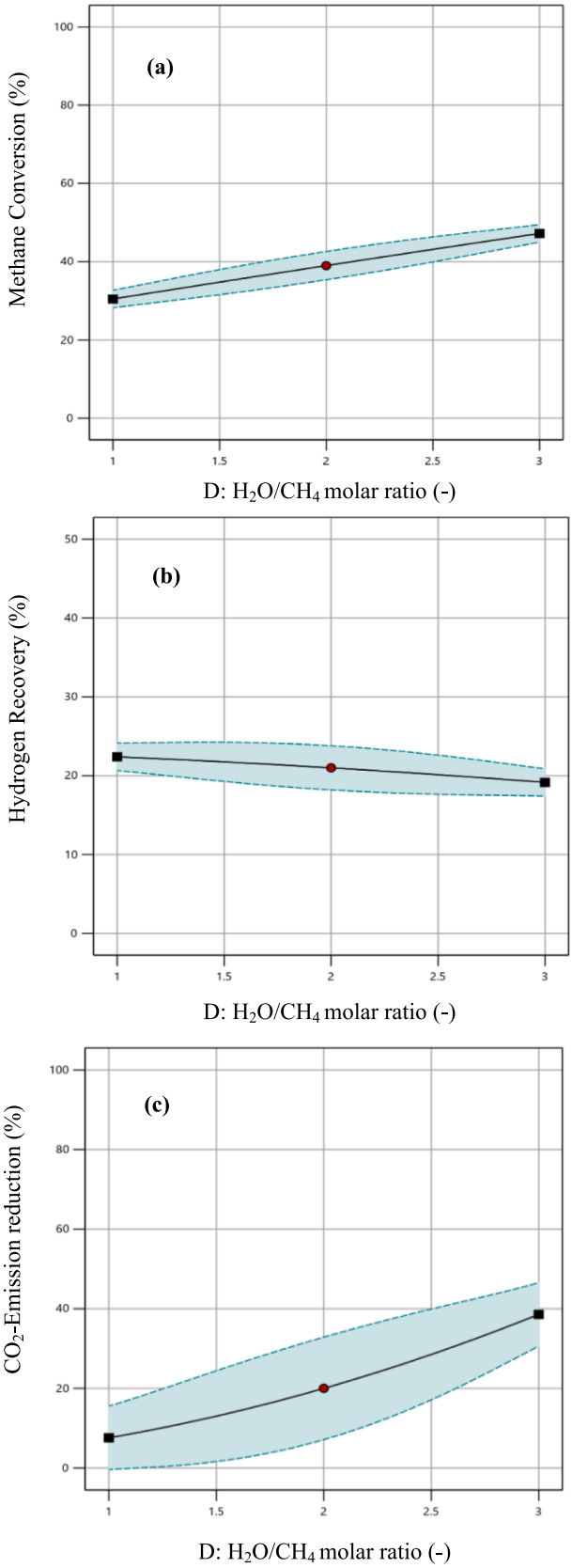

Fig. 7. A) ch_4 conversion, b) H_2 recovery, and c) CO_2 emission reduction versus feed molar ratio (H_2O/CH_4) at reaction pressure = 4 bar, reaction temperature = 673 K, GHSV = 9000 h^{-1}, and S/F = 5.

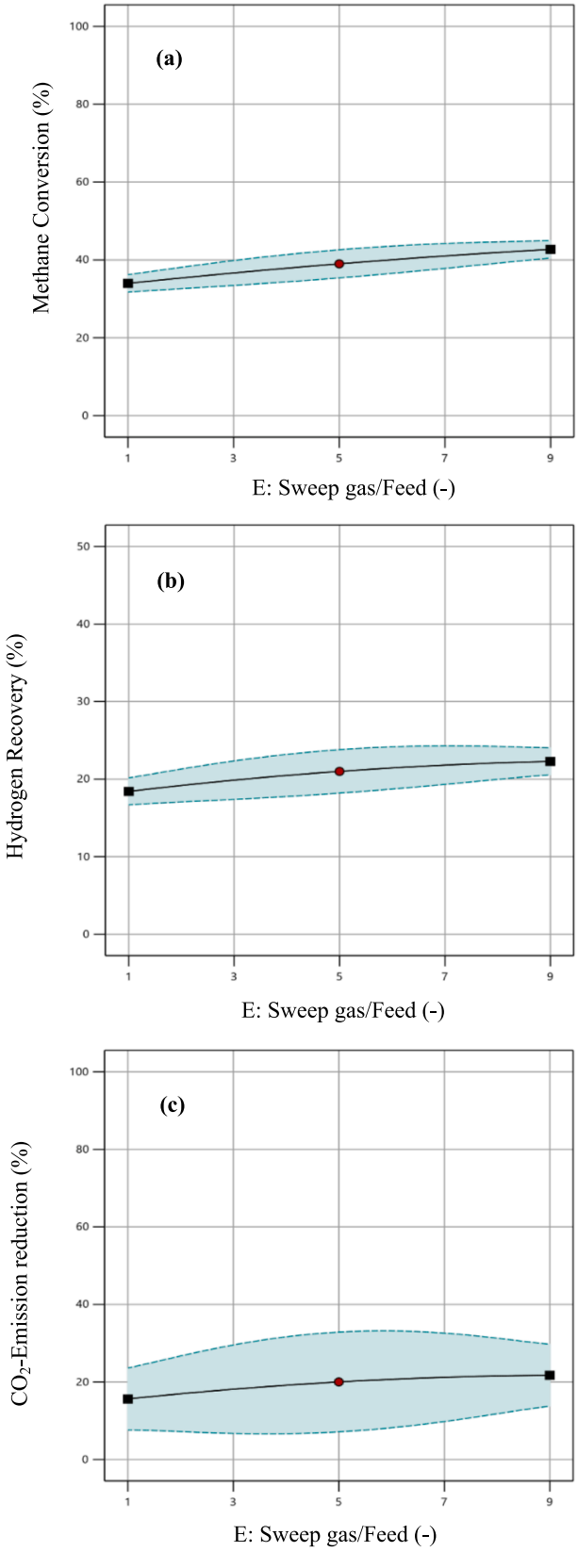

Fig. 8. A) ch_4 conversion, b) H_2 recovery and c) CO_2 emission reduction versus sweep gas ratio (S/F)(at reaction pressure = 4 bar, reaction temperature = 673 K, GHSV = 9000 h^{-1}, and H_2O/CH_4 = 2).

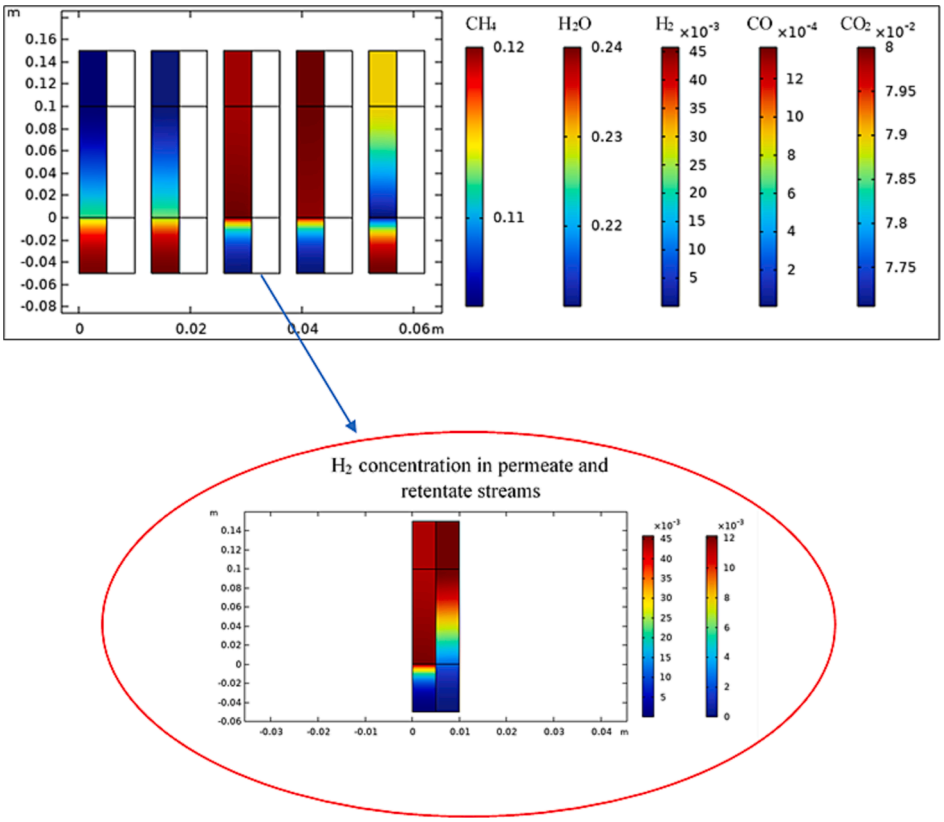

Fig. 9. Concentration distribution of components obtained by 2D-CFD simulations in Pd-Ag MR during BSR reaction.

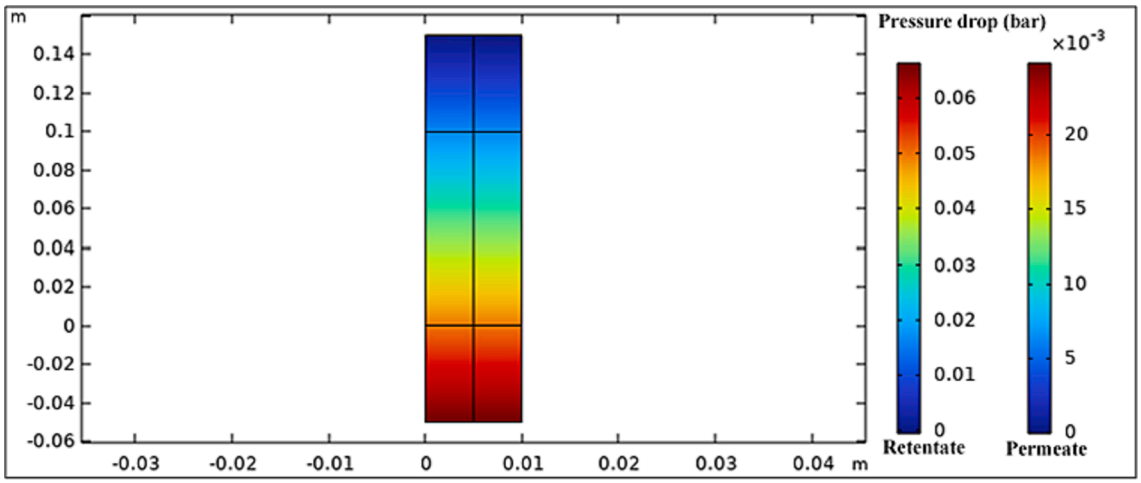

Fig. 10. Pressure distribution in Pd-Ag MR during BSR reaction.

Numerical response optimization helps to identify factor settings that meet the desired criteria efficiently [32].

The optimal conditions achieved using the CFD-RSM method were a reaction temperature of 683 K, a reaction pressure of 6 bar, a GHSV of 3000 h^{-1}, $H_2O/CH_4 = 1.34$, and S/F equal to 9, resulting in maximum CH_4 of 100 %, H_2 recovery of 43 %, and CO_2 emission reduction of 81 %. The 2D response surface analysis presented in Fig. 11 further confirmed the attainment of optimal parameters.

5. Conclusion and future trends

In summary, this study developed comprehensive 2D-CFD models incorporating detailed chemistry and transport aspects to simulate BSR within a Pd-Ag MR for decarbonized hydrogen production. These models underwent validation against experimental data coming from our previous study [6]. Employing a parametric study, the influence of reaction temperature, reaction pressure, GHSV, H_2O/CH_4 ratio, and sweep gas ratio (S/F) on key performance indicators - namely CH_4 conversion, H_2 recovery, and CO_2 emission reduction - was thoroughly investigated. Within the examined range of parameters, an increase in temperature had the most significant impact on increasing the key performance indicators, while the effect of increasing the sweep gas ratio was not so impacting on the MR performance. Additionally, an increase in GHSV had an inverse effect, leading to a reduction in all three output parameters. The pioneeristic integration of RSM with the CFD method realized in this work facilitated efficient optimization, revealing

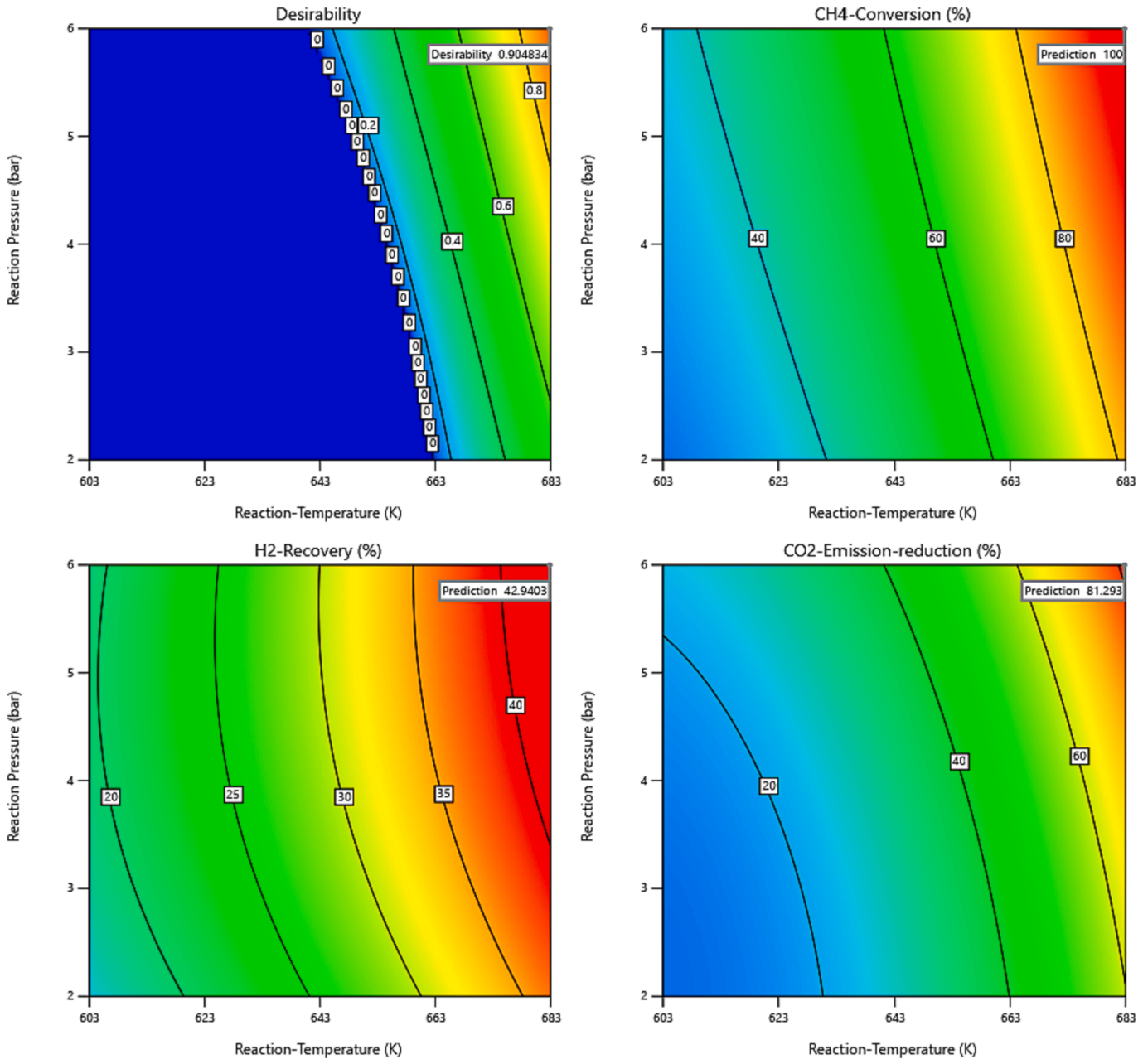

Fig. 11. The 2D response surface contours for CH_4 conversion, H_2 recovery and CO_2 emission reduction (Reaction temperature and reaction pressure values effects).

critical parameters that significantly impact system performance. Under optimized conditions, the system achieved complete CH_4 conversion, 43 % H_2 recovery, and 81 % CO_2 emissions reduction at a reaction temperature of 683 K, reaction pressure of 6 bar, GHSV of 3000 h^{-1}, H_2O/CH_4 ratio of 1.34, and a sweep gas ratio of 9. This study underscores that the combined CFD-RSM approach not only mitigates the need for costly and time-consuming experimental work but also provides highly accurate and practical information, crucial for the design of MR systems utilized for hydrogen production during the BSR process.

CRediT authorship contribution statement

K. Ghasemzadeh: Writing – review & editing, Supervision, Conceptualization. **T. Torabi:** Investigation, Data curation. **T. Yousefi Amiri:** Investigation, Data curation. **A. Fortunelli:** Visualization, Methodology, Conceptualization. **A. Iulianelli:** Writing – review & editing, Validation, Funding acquisition.

Declaration of competing interest

The authors declare that they have no known competing financial interests or personal relationships that could have appeared to influence the work reported in this paper.

Data availability

Data will be made available on request.

Acknowledgements

This work received funds from the European Union – NextGeneration EU from the Italian Ministry of Environment and Energy Security POR H2 AdP MMES/ENEA with involvement of CNR and RSE, PNRR - Mission 2, Component 2, Investment 3.5 “Research and development on hydrogen” - WP1.2 - LA1.2.7: “Development of biomass gasification

processes, biogas reforming and integrated processes to produce hydrogen for stationary applications and validation in prototype reactors" - CUP: B93C22000630006.

References

[1] Vita A, Pino L, Cipitì F, Laganà M, Recupero V. Biogas as renewable raw material for syngas production by tri-reforming process over $NiCeO_2$ catalysts: optimal operative condition and effect of nickel content. Fuel Proc Techn. 2014;127:47–58.

[2] Paturzo L, Basile A, Iulianelli A, Jansen JC, Gatto I, Passalacqua E. High temperature proton exchange membrane fuel cell using a sulfonated membrane obtained via H_2SO_4 treatment of PEEK-WC. Catal Today 2005;104:213–8.

[3] Dincer I. Covid-19 coronavirus: closing carbon age, but opening hydrogen age. Int J Energy Res. 2020;44:6093–7.

[4] Basile A, Iulianelli A. Advances in Hydrogen Production, Storage and Distribution. 1st ed. Woodhead Publishing; 2014. p. 1–546. https://doi.org/10.1016/C2013-0-16359-3. ISBN: 9780857097682.

[5] Nikolaidis P, Poullikkas A. A comparative overview of hydrogen production processes. Renew Sustain Energy Rev. 2017;67:597–611.

[6] Iulianelli A, Brunetti A, Pino L, Italiano C, Ferrante GD, Gensini M, et al. An integrated two stages inorganic membrane-based system to generate and recover decarbonized H_2: an experimental study and performance indexes analysis. Renew Energy. 2023;210:472–85.

[7] Tuna CE, Silveira JL, da Silva ME, Boloy RM, Braga LB, Pérez NP. Biogas steam reformer for hydrogen production: evaluation of the reformer prototype and catalysts. Int J Hydrogen En. 2018;43:2108–20.

[8] Ghasemzadeh K, Morrone P, Iulianelli A, Liguori S, Babaluo AA, Basile A. H_2 production in silica membrane reactor via methanol steam reforming: modeling and HAZOP analysis. Int J Hydrogen Ener. 2013;38:10315–26.

[9] Meloni E, Iervolino G, Ruocco C, Renda S, Festa G, Martino M, et al. Electrified hydrogen production from methane for PEM fuel cells feeding: a review. Energies. 2022;15:3588.

[10] Iulianelli A, Manisco M, Bion N, Le Valant A, Epron F, Colpan CO, et al. Sustainable H_2 generation via steam reforming of biogas in membrane reactors: H_2S effects on membrane performance and catalytic activity. Int J Hydrogen En. 2021;46:29183–97.

[11] Chouhan K, Sinha S, Kumar S, Kumar S. Simulation of steam reforming of biogas in an industrial reformer for hydrogen production. Int J Hydrogen E. 2021;46:26809–24.

[12] Zheng S, Liu H, Li D, Liu Z, Zhou B, Lu Q. Effects of radiation reabsorption on the laminar burning velocity of methane/air and methane/hydrogen/air flames at elevated pressures. Fuel. 2022;311:122586.

[13] Sirkar KK, Fane AG, Wang R, Wickramasinghe SR. Process intensification with selected membrane processes. Chem Eng Proc Process Intens. 2015;87:16–25.

[14] Amiri TY, Ghasemzadeh K, Iulianelli A. Membrane reactors for sustainable hydrogen production through steam reforming of hydrocarbons: a review. Chem Eng Proc Process Intens. 2020;157:108148.

[15] Di Marcoberardino G, Foresti S, Binotti M, Manzolini G. Potentiality of a biogas membrane reformer for decentralized hydrogen production. Chem Eng Proc Process Intens. 2018;129:131–41.

[16] Rahimpour MR, Samimi F, Babapoor A, Tohidian T, Mohebi S. Palladium membranes applications in reaction systems for hydrogen separation and purification: a review. Chem Eng Proc Process Intens 2017;121:24–49.

[17] Castillo JMV, Sato T, Itoh N. Effect of temperature and pressure on hydrogen production from steam reforming of biogas with Pd–Ag membrane reactor. Int J Hydrogen E. 2015;40:3582–91.

[18] Parente M, Soria M, Madeira LM. Hydrogen and/or syngas production through combined dry and steam reforming of biogas in a membrane reactor: a thermodynamic study. Renew Energy. 2020;157:1254–64.

[19] Zawawi MH, Saleha A, Salwa A, Hassan N, Zahari NM, Ramli MZ, et al. A review: fundamentals of computational fluid dynamics (CFD), AIP conference proceedings. AIP Publish 2018;2030(1):020252. https://doi.org/10.1063/1.5066893.

[20] Abadi AF, Kazemeini M, Ekramipooya A. Investigating a HEX membrane reactor for CO_2 methanation using a Ni/Al_2O_3 catalyst: A CFD study. Int J Hydrogen Ener 2023;48:25075–91.

[21] Bian Z, Xia H, Zhong W, Jiang B, Yu Y, Wang Z, et al. CFD simulation on hydrogen-membrane reactor integrating cyclohexane dehydrogenation and CO_2 methanation reactions: a conceptual study. Energy Conv Manag 2021;235:113989.

[22] Choi H, Kim SH, Bae J, Katikaneni SPR, Jamal A, Harale A, et al. CFD analysis and scale up of a baffled membrane reactor for hydrogen production by steam methane reforming. Computers Chem Eng. 2022;165:107912.

[23] Bian Z, Xia H, Jiang B, Wang Z, Yu Y, Yu K, et al. A CFD study on H_2-permeable membrane reactor for methane CO_2 reforming: effect of catalyst bed volume. Int J Hydrogen Ener. 2021;46:38336–50.

[24] Ghasemzadeh K, Harasi NJ, Iulianelli A, Basile A. Theoretical evaluation of various configurations of silica membrane reactor in methanol steam reforming using CFD method. Int J Hydrogen Ener 2020;45:7354–63.

[25] Yu Y, Bian Z, Tan W, Zhong Q. CFD modelling and simulation of a zeolite catalytic membrane reactor for low temperature water-gas shift reaction. Chem Eng Processing Process Intensif. 2022;178:108994.

[26] Ghasemzadeh K, Ghahremani M, Amiri TY, Basile A. Performance evaluation of Pd-Ag membrane reactor in glycerol steam reforming process: development of the CFD model. Int J Hydrogen Ener. 2019;44:1000–9.

[27] Ghasemzadeh K, Khosravi M, Tilebon SS, Aghaeinejad-Meybodi A, Basile A. Theoretical evaluation of Pd-Ag membrane reactor performance during biomass steam gasification for hydrogen production using CFD method. Int J Hydrogen Ener 2018;43:11719–30.

[28] Cipitì F, Barbera O, Briguglio N, Giacoppo G, Italiano C, Vita A. Design of a biogas steam reforming reactor: a modelling and experimental approach. Int J Hydrogen Ener 2016;41:11577–83.

[29] Hajjaji N, Martinez S, Trably E, Steyer JP, Helias A. Life cycle assessment of hydrogen production from biogas reforming. Int J Hydrogen Ener 2016;41:6064–75.

[30] De Rosa F, Smyth B, McCullough G, Goguet A. Using multi-criteria and thermodynamic analysis to optimize process parameters for mixed reforming of biogas. Int J Hydrogen Ener. 2018;43:18801–13.

[31] Caldas GLR, Mattos LV, Moreira RM. Scale-up analysis of hydrogen rich-stream production from biogas reforming in membrane reactors using numerical modeling. Int J Hydrogen Ener. 2023;48:25197–215.

[32] Jabbari B, Jalilnejad E, Ghasemzadeh K, Iulianelli A. Modeling and optimization of a membrane gas separation based bioreactor plant for biohydrogen production by CFD–RSM combined method. J Water Process Eng. 2021;43:102288.

[33] Awad AM, Hussein IA, Nasser MS, Ghani SA, Mahgoub AO. A CFD-RSM study of cuttings transport in non-Newtonian drilling fluids: impact of operational parameters. J Petroleum Sci Eng 2022;208:109613.

[34] Banik A, Biswal SK, Bandyopadhyay TK. Predicting the optimum operating parameters and hydrodynamic behavior of rectangular sheet membrane using response surface methodology coupled with computational fluid dynamics. Chem Papers. 2020;74:2977–90.

[35] Solangi ZA, Bhatti I, Qureshi K. A combined CFD-response surface methodology approach for simulation and optimization of arsenic removal in a fixed bed adsorption column. Processes. 2022;10:1730.

[36] Xu J, Froment GF. Methane steam reforming, methanation and water-gas shift: I. Intrinsic kinetics, AIChE J. 1989;35:88–96.